Partitioning of Nonspherical Molecules between Bulk Solution and Porous Solids

Monte Carlo simulation is used to calculate partition coefficients for rigid, axisymmetric, nonspherical molecules in various pore geometries. Novel quantitative results are presented for a variety of molecule and pore shapes, including pores of nonuniform cross-section such as the interstitial space within granular and fibrous materials.

Quick estimation methods for obtaining partition coefficients are discussed, and the effects of molecule and pore wall curvature are described in detail. A boundary perturbation analysis is used to derive easy-to-use formulas for a variety of molecule shapes in circular pores.

Kirk W. Limbach
Johannes M. Nitsche
James Wei
Department of Chemical Engineering
Massachusetts Institute of Technology
Cambridge, MA 02139

Introduction

The partitioning of rigid molecules between bulk solution and porous solids is an important aspect of hindered diffusion (Anderson and Quinn, 1974; Brenner and Gaydos, 1977; Baltus and Anderson, 1983; Deen, 1987) and related topics, such as ultrafiltration (Ferry, 1936; Renkin, 1954), gel permeation chromatography (Porath, 1963; Giddings et al., 1968; Cheng, 1986), and osmotic flow in membranes (Anderson and Malone, 1974; Anderson, 1981). Analytical and numerical partitioning results, therefore, have immediate applicability to a variety of transport processes in biology and engineering.

The partition coefficient, Φ, is the equilibrium ratio of solute concentration within the interstitial space of a porous material to that in the bulk solution. In the dilute solution limit, to which we restrict our attention, the effects of solute-solute interactions are negligible. For the case of a dilute solution in a neutral pore, no attractive forces exist between the molecule and pore wall, where Φ is expressed as the ratio of orientation-averaged pore volume accessible to the molecule center to the total pore volume.

Giddings et al. (1968) introduced two parameters that characterize molecule and pore size. Molecules may be described by an orientation-averaged projected length, which we denote the mean projected molecule radius, r_m. Pores may be described by their hydraulic radius, $(V/S)_p$, which is the ratio of pore volume to surface area, and the ratio $r_m/(V/S)_p$ is defined as λ. The mean projected radius for axisymmetric molecules may be expressed as:

$$r_m = \frac{1}{2}\int_0^\pi h \sin\theta \, d\theta, \tag{1}$$

where h is the closest possible approach of the molecule center to a fixed flat surface (cf Baltus and Anderson, 1984). The approach, h, will vary with θ, the angle between the axis of rotation of the molecule and the surface's normal vector. The mean projected radius, although not directly measurable, may be related to the Stokes-Einstein radius of the molecule (Baltus and Anderson, 1984). The Stokes-Einstein radius can be experimentally determined through bulk diffusion measurements.

The partition coefficient exhibits the asymptotic behavior

$$\Phi \approx 1 - \lambda \tag{2}$$

as λ approaches zero for any molecule and pore shapes. In this limit, a molecule near the pore wall "sees," to first approximation, a flat surface. The orientation-averaged thickness of the layer to which the molecule center is sterically excluded is therefore r_m, and the fractional pore volume excluded from the molecule center is λ, hence Eq. 2.

The partitioning behavior of small molecules in neutral porous networks can be estimated from Eq. 2, which accounts for the leading-order effects of molecule and pore size. Higher-order effects may be elucidated through a boundary perturbation analysis. This analysis is demonstrated below for several molecule shapes in circular pores and could in principle be extended to describe other molecule-porous network systems. The analysis is strictly valid for small λ or Φ near unity, but was found to be accurate at all but relatively small Φ. Geometric partitioning problems of any complexity may be accurately described at all λ's by the Monte Carlo technique developed here.

In practice, partition coefficients for various rigid molecule-porous network systems may be estimated through the use of model pores on an equal λ basis. Partitioning in equilateral triangular pores, in 60° rhombic pores and within close-packed

Correspondence concerning this paper should be addressed to K. W. Limbach.

granular materials, for instance, could be estimated for all but large molecules by partitioning in an equivalent circular cylindrical pore.

Cylindrical model pores, however, may be inappropriate for many practical applications where a myriad of complex pore shapes might be encountered. We therefore consider three relatively simple cases of partitioning in pores of nonuniform cross-section that may be used as models for more complicated systems.

The interstitial space between corrugated sinusoidal plates is considered to demonstrate the appearance of a molecule cutoff size and the effect of pore wall tortuosity for nonspherical molecules. The molecule cutoff size is reached when molecules which might otherwise fit in the body of a pore are excluded from the pore because they are too large to pass through the pore throat.

The more directly applicable cases of partitioning in granular materials and fibrous networks are also considered and demonstrate the effects of pore wall curvature. Pore wall curvature may be "predominantly concave" or "predominantly convex." Partitioning in "convex-pore" systems, such as sparse fibrous networks, is fundamentally different from that in "concave-pore" systems, such as dense fibrous networks or ordinary capillaries. The partitioning curve has a negative second derivative, $d^2\Phi/d\lambda^2$, in the first case, and a positive second derivative in the second case.

Background

The calculation of partition coefficients for rigid spherical solutes in circular pores, assuming only steric solute pore wall interactions, has been considered by Pappenheimer et al. (1951), who presented the following expression based on geometric arguments:

$$\Phi = (1 - \lambda_a)^2, \tag{3}$$

where λ_a is the ratio of sphere to pore radius. Equation 3 describes Φ as the ratio of the pore area available to the center of the diffusing solute and the entire pore area. Subsequent investigations for spherical molecules have addressed molecule-pore wall interactions (cf Giddings et al., 1968), including electrical double-layer effects (Malone and Anderson, 1978; Smith and Deen 1983), as well as appreciable solvent molecule size (Solomon, 1968; Satterfield et al., 1973).

In this paper, we consider the partitioning of rigid nonspherical molecules, for which the only extensive analysis is that of Giddings et al. (1968). They established a general foundation for partitioning from the principles of statistical thermodynamics. The partition coefficient may be expressed as the ratio of the configurational integrals:

$$\Phi = \frac{\int_{\underline{x}} \int_{\underline{\phi}} P(\underline{x}, \underline{\phi})\, d^3\underline{x}\, d^3\underline{\phi}}{\int_{\underline{x}} \int_{\underline{\phi}} d^3\underline{x}\, d^3\underline{\phi}}. \tag{4}$$

Integration is over the set of all molecule center positions $\underline{x}$ lying within the pore space and all molecule orientations $\underline{\phi}$. The numerator of Eq. 4 represents the integration of the probability density, $P(\underline{x}, \underline{\phi})$, of the molecule having a given configuration $(\underline{x}, \underline{\phi})$. When any portion of the molecule does not lie within the pore space, the configuration is not allowed and $P(\underline{x}, \underline{\phi})$ is zero. The denominator is the corresponding integration over an identical configurational space, but evaluated for the bulk liquid, where $P(\underline{x}, \underline{\phi})$ is, by definition, unity. The probability density, $P(\underline{x}, \underline{\phi})$, is a function of molecule and pore shape, size, and molecule-pore interactions.

Molecule-pore interactions may include long-range attractive or repulsive forces. For the special case of purely steric interactions, $P(\underline{x}, \underline{\phi})$ is unity for all configurations in which the molecule does not touch the pore wall and zero for disallowed configurations. This simplification reduces the calculation of Φ to a geometric problem, where Φ is the ratio of the orientation-averaged pore volume available to the molecule center to total pore volume.

The purely steric case, although reducible to geometric terms, comprises the most difficult conceptual aspect of nonspherical molecule partitioning. Inclusion of other interactions may be accomplished by inserting the appropriate Boltzman distribution for $P(\underline{x}, \underline{\phi})$ into the numerator of Eq. 4 (Giddings et al., 1968).

Pores of uniform cross-section

Giddings et al. (1968) studied partitioning of axisymmetric molecules in inert rectilinear pores using the above-mentioned geometric arguments. The partition coefficient was expressed as the orientationally-averaged pore area accessible to the molecule center divided by the total pore cross-sectional area:

$$\Phi = \frac{\int_0^{\pi} \int_0^{\pi/2} F_p \sin\theta\, d\theta\, d\phi}{\int_0^{\pi} \int_0^{\pi/2} \sin\theta\, d\theta\, d\phi}, \tag{5}$$

where θ is the angle between the pore and molecule axes, ϕ is the azimuthal angle, and F_p is the fraction of the pore area accessible to the center of the molecule at a given orientation. In circular pores, F_p is independent of ϕ and Eq. 5 reduces to

$$\Phi = \int_0^{\pi/2} F_p \sin\theta\, d\theta. \tag{6}$$

Equation 6 was employed by Giddings et al. (1968) to describe the partition coefficient for ellipsoids of revolution (spheroids). Unfortunately, their resulting double integral is cumbersome and must be evaluated numerically. It should be noted that their integral is off by a factor of $4/\pi$; the correct equation is:

$$\Phi = (4/\pi) \int_0^1 d\alpha \int_0^{\pi/2} d\theta \sin\theta (1 - \alpha^2)^{1/2} \times \left[1 - \frac{(\lambda_a^2 - \lambda_b^2)\cos^2\theta + \lambda_b^2}{[\lambda_a^2\alpha^2 + [(\lambda_a^2 - \lambda_b^2)\cos^2\theta + \lambda_b^2](1 - \alpha^2)]^{1/2}}\right] \times \left[1 - \frac{\lambda_a^2[(\lambda_a^2 - \lambda_b^2)\cos^2\theta + \lambda_b^2]}{[\lambda_a^2\alpha^2 + [(\lambda_a^2 - \lambda_b^2)\cos^2\theta + \lambda_b^2](1 - \alpha^2)]^{3/2}}\right], \tag{7}$$

where a is the radius of the ellipsoid, b is the half axial length, α is the ratio of a radial coordinate to the ellipsoid radius, λ_a is the ratio of the ellipsoid radius to the pore radius, a/R, λ_b is b/R, and the integrand is taken as zero when either of the multipli-

cands in parenthesis is negative or

$$0 > 1 - \frac{\lambda_a^2}{\{\lambda_a^2\alpha^2 + [(\lambda_a^2 - \lambda_b^2)\cos^2\theta + \lambda_b^2](1 - \alpha^2)\}^{1/2}} \quad (8)$$

The ratio of ellipsoid primary dimensions b/a is very small for a disk-like ellipsoid, unity for a sphere, and very large for a thin rod. For later convenience we define

$$\gamma = b/a \quad (9)$$

Giddings et al. (1968) developed an analytical expression for infinitely thin rods in circular pores. This equation, given in its correct form below, has a sign error in the original publication.

$$\Phi = 1 - \frac{4[\{1 + \lambda_b^2\}E(\pi/2, \lambda_b) - \{1 - \lambda_b^2\}F(\pi/2, \lambda_b)]}{3\pi\lambda_b} \quad (\lambda_b \le 1)$$

$$\Phi = 1 - \frac{8}{3\pi} \quad (\lambda_b = 1)$$

$$\Phi = 1 - \frac{4[\{1 + \lambda_b^2\}E(\pi/2, 1/\lambda_b) - \{\lambda_b^2 - 1\}F(\pi/2, 1/\lambda_b)]}{3\pi} \quad (\lambda_b \ge 1) \quad (10)$$

with F and E the elliptical integrals of the first and second kind, respectively.

The case of capsule-shaped molecules, those having hemispherical ends and a circular cylindrical body, was also considered. Capsule partitioning was calculated indirectly from the thin rod case by simply encapsulating the rod in a layer of given thickness, increasing the pore radius by this same thickness and then recognizing that the partition coefficient of the resulting capsule-shaped molecule and larger pore is related to that of the original rod and pore.

The partitioning of molecules in noncircular cylindrical pores has been considered by Giddings et al. (1968), Malone and Anderson (1978), and Glandt (1981). A comprehensive review of the effects of pore shape on partitioning was given by Deen (1987).

Nonuniform pores

The published data on partitioning in nonrectilinear pores include: the random-fiber analysis of Ogsten (1958) and Laurent and Killander (1964); and the analyses of random sphere media by van Kreveld and van den Hoed (1973), Rikvold and Stell (1985), and Cheng (1986). All of these investigations are restricted to spherical molecules. Giddings et al. (1968) considered partitioning of nonspherical particles in random plane and random fiber pore models, but their analysis can unambiguously furnish only the leading order effects of molecule and pore size.

Monte Carlo Simulation

Monte Carlo simulation was tested by comparison with numerical results derived from Eqs. 7 and 8, and then used to determine the partition coefficients for additional molecule or pore shapes not easily amenable to analytical consideration. The technique used was similar to that of Davidson et al. (1987) who addressed partitioning of freely-jointed chains in circular pores.

The partitioning of axisymmetric molecule shapes, including ellipsoids of revolution, circular cylinders, and hemispheres, was simulated in circular, triangular, rhombic and parallel-plate pores. Spherical and rod-shaped molecules were simulated in pores of nonuniform cross-section.

The partition coefficient, Φ, was determined by comparing the concentration of molecules within the pore to that in an equivalent volume of bulk solution. Pore shape and size were first selected and the pore wall location was determined. After selecting a molecule size and shape, molecule location and orientation were randomly chosen a total of up to 100,000 times in each simulation. The orientation vector was selected randomly in a spherical domain to insure an equal probability of all molecule orientations in three-dimensional space. For each trial of a specific location and orientation, the molecule boundary was compared with that of the pore, Figure 1. The partition coefficient was calculated as the ratio of the number of trials in which the entire molecule lay within the pore boundary to the number of trials in which the molecule center lay within the pore boundary.

Axisymmetric molecule shapes were described by up to 762 points on the molecule surface. Molecules were sectioned into 21 equally-spaced circular slices or discs. Each disc was represented by up to 40 points along its perimeter, and the disc radius was calculated according to the desired molecule shape.

Program efficiency was improved by dividing the pore into three regions: a central region in which the entire molecule must lie within the pore; an outer region in which the entire molecule cannot lie within the pore; and an intermediate region for which the location of the molecule's surface must be calculated to determine if the molecule surface penetrates through the pore wall. The time-consuming numerical generation of the molecule surface is necessary only in the intermediate region.

Simulation accuracy was determined by comparing Monte Carlo results with numerical results calculated by independent means. Figure 2 compares simulation results for ellipsoids of revolution in circular pores to those calculated by numerical

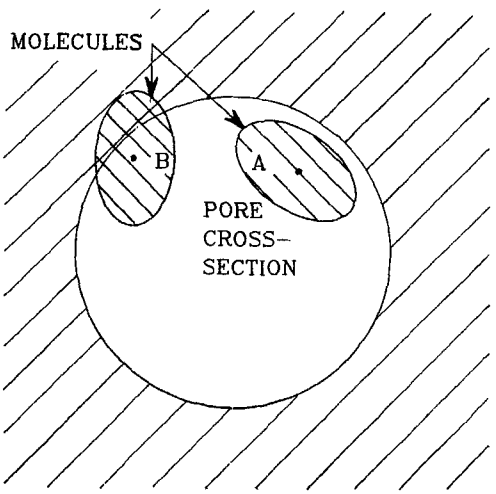

Figure 1. Comparison of molecule and pore wall location.

In Monte Carlo simulation, molecule A is included in both the bulk and pore concentrations. Molecule B is included only in the bulk concentration.

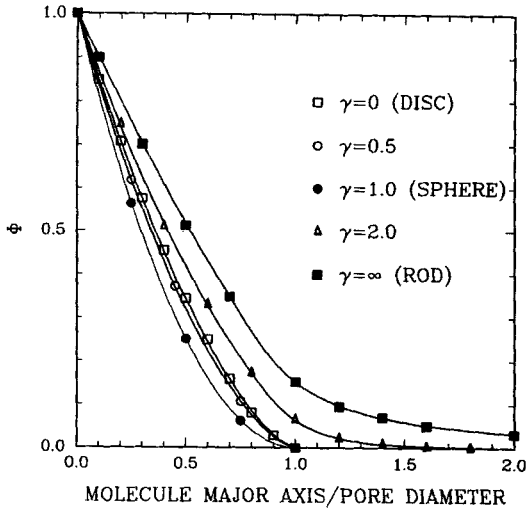

Figure 2. Ellipsoid of revolution partitioning in circular pores.

Monte Carlo results, given as points, are compared to numerical results, given as lines, which are based on the theory of Giddings et al. (1968).

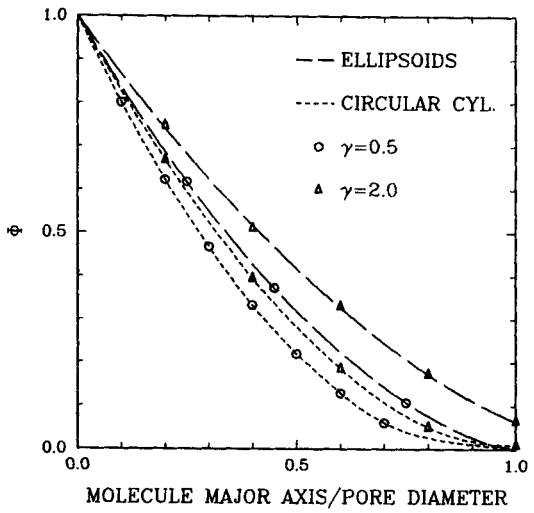

Figure 3. Comparison of ellipsoid and circular cylinder-shaped molecule partitioning in circular pores by Monte Carlo simulation.

integration of Eqs. 7 and 8 given by Giddings et al. (1968). The average error of simulated values was less than 1%.

Simulation precision may be determined through statistical analysis. Davidson et al. (1987) estimated the precision of their partitioning results using binomial statistics and found the local error to be roughly proportional to the inverse square root of the number of successful partitioning trials at a given radial position in the pore. A trial is successful when the entire molecule is found to lie within the pore boundary. Since the ratio of successful to total simulation trials decreases as molecule size increases, we increased the total number of trials with the ratio of molecule to pore size in order to maintain the precision of simulation results.

New partitioning results include those for circular cylindrical and hemisphere-shaped molecules, triangular pores, nonspherical molecules in rhombic and parallel-plate pores, and spherical and rod-shaped molecules in various pores of nonuniform cross-section. Some results of current interest are presented below in an easily used form. A more detailed discussion of partitioning trends will follow.

Molecule shape is a crucial element in the determination of partitioning. To illustrate this we consider ellipsoid and circular cylinder-shaped molecule partitioning in circular pores. Figure 3 demonstrates that circular cylinders would have a substantially lower Φ than ellipsoids of the same dimension. It is difficult to determine the true shape of an actual molecule; however, the best way to accomplish this in some cases is to bound Φ of a molecule between two extremes. A related example of current interest is the partitioning of porphyrins and polyaromatic compounds which have been described as disc-like (Baltus and Anderson, 1984) and might be bound by the cases of oblate spheroids and short cylindrical rods.

The development of track etched mica membranes has created interest in hindered diffusion through rhombic pores (Glandt, 1981; Baltus and Anderson, 1983; Deen, 1987). Figure 4 describes the limiting cases for partitioning of ellipsoids of revolution in 60° rhombic pores.

The partition coefficient for ellipsoids of revolution in parallel-plate pores is shown in figure 5. The hydraulic radius $(V/S)_p$, of parallel-plate pores is one half the separation distance between the plates. Parallel-plate pores are unique in that the pore wall has no curvature. For this reason, molecules with a maximum projected length smaller than the plate spacing are only subject to leading order partitioning effects, described by Eq. 2, hence the linear region in Figure 5.

Additional results are summarized in Figures 6 and 7, which describe Φ as a function of λ. Figure 6 describes the partitioning of various shaped molecules in circular pores, and Figure 7 describes the effect of pore shape on spherical molecule partitioning. Estimating partition coefficients in practice might be accomplished by modeling actual systems with a molecule-pore combination of equal λ (Giddings et al., 1968). These figures illustrate the importance of selecting the appropriate model system and provide a quantitative measure of possible deviation from the model.

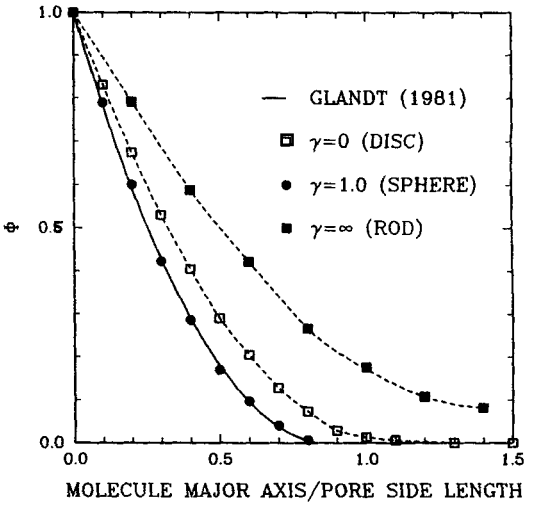

Figure 4. Monte Carlo results, given as points, for ellipsoid of revolution partitioning in a 60° rhombic pore.

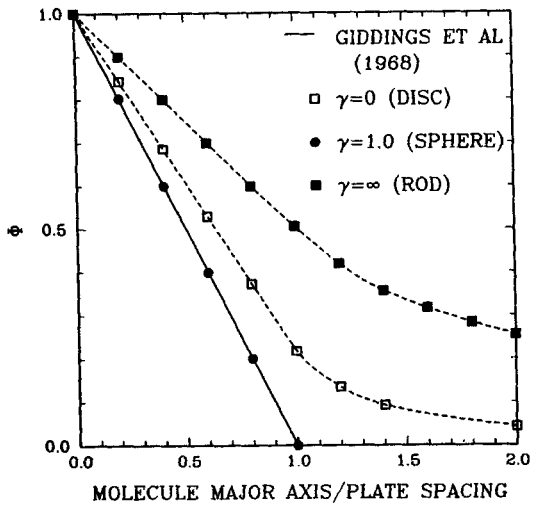

Figure 5. Monte Carlo results, given as points, for ellipsoid of revolution partitioning in parallel-plate pores.

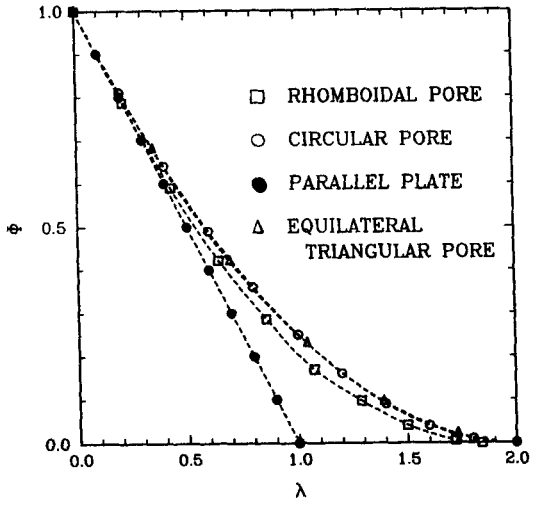

Figure 7. Effect of the pore shape on the partitioning of spherical molecules. Monte Carlo results are given as points.

Boundary Perturbation Analysis for Small Molecules

The Monte Carlo algorithm described above represents an efficient, general method of calculating partition coefficients, and may be applied when the geometrical configurations become extremely complicated. For certain relatively simple molecule-pore combinations, it is possible to supplement detailed simulations with analytical formulas that represent the numerical results accurately over certain ranges of λ, thus partially eliminating the need for interpolation between limited amounts of numerical "data." In this section, we use a perturbation analysis to derive formulas for the partition coefficient of the form:

$$\Phi = 1 + \Phi_1\lambda_i + \Phi_2\lambda_i^2 + O(\lambda_i^3)$$

for spheroids, hemispheres and circular cylinders in circular cylindrical pores in the limit $\lambda_i \ll 1$, where λ_i denotes either λ_a or λ_b. These formulas are shown to agree with the simulation results for surprisingly large values of λ_i.

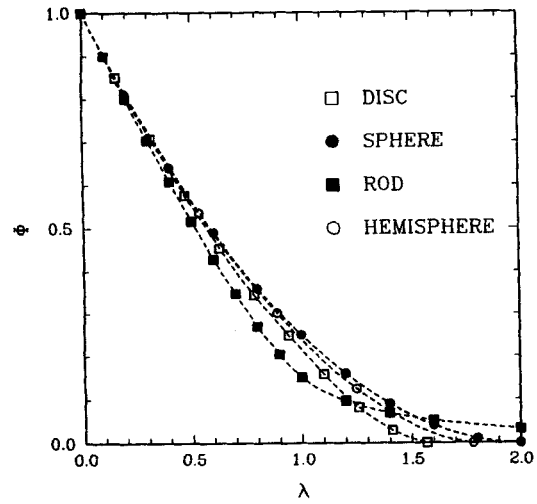

Figure 6. Effect of molecule shape on partitioning in a circular cylindrical pore. Monte Carlo results are given as points.

Oblate spheroids

The projection of a spheroid, with radius a and half axial length b, onto a plane perpendicular to the pore axis is an ellipse with semiaxes a and $[a^2\cos^2\theta + b^2\sin^2\theta]^{1/2}$. Since the area fraction F_p is independent of ϕ (Giddings et al., 1968), it suffices to compute F_p for a particular value of ϕ, say $\phi = \pi/2$. Then, as shown in Figure 8, the projected ellipse has horizontal semiaxis a and vertical semiaxis aC, where we have defined

$$C = \frac{\text{vertical semiaxis}}{\text{horizontal semiaxis}} = [\cos^2\theta + (b/a)^2\sin^2\theta]^{1/2}. \quad (11)$$

The set of points accessible to the center of the projected ellipse is bounded by the dashed curve $\mathcal{L}$ in Figure 8 corresponding to tangential contact of the ellipse with the circular

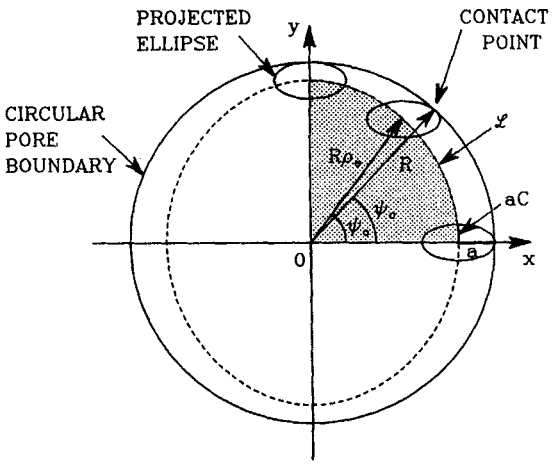

Figure 8. Geometrical construction for calculating the area fraction F_p for oblate spheroids.

pore boundary. Working with cartesian coordinates, Giddings et al. (1968) derived the integral formula 7 for the partition coefficient for spheroids, which requires the area inside $\mathcal{L}$ to be determined numerically. The approach taken here is to obtain an explicit equation for $\mathcal{L}$ in the form of a perturbation series in powers of $\lambda_a = a/R$ for small λ_a and then to carry the analysis through to obtain a corresponding perturbation expansion for the partition coefficient Φ.

We utilize polar coordinates (r, ψ) instead of Cartesian coordinates (x, y). With (r_0, ψ_0) denoting the polar coordinates of its center, the projected ellipse is given by:

$$f(r, \psi; r_0, \psi_0) = C^2(r\cos\psi - r_0\cos\psi_0)^2 + (r\sin\psi - r_0\sin\psi_0)^2 - a^2C^2 = 0.$$

Curve $\mathcal{L}$ corresponds to the situation in which the projected ellipse just touches the circular pore boundary at some contact point (r_c, ψ_c). Thus, at $(r, \psi) = (r_c, \psi_c)$, the following conditions must be satisfied:

$$r = R \quad \text{(contact point lies on circle)},$$

$$f(r, \psi; r_0, \psi_0) = 0 \quad \text{(contact point lies on ellipse)},$$

$$\frac{dr}{d\psi}(r, \psi; r_0, \psi_0)\Big|_{\text{ellipse}} = 0 \quad \text{(tangency at contact point)}.$$

These conditions lead to the two equations:

$$C^2(\cos\psi_c - \rho_0\cos\psi_0)^2 + (\sin\psi_c - \rho_0\sin\psi_0)^2 = C^2\lambda_a^2, \quad (12)$$

$$\rho_0 = (1 - C^2)\sin\psi_c\cos\psi_c/(\sin\psi_0\cos\psi_c - C^2\sin\psi_c\cos\psi_0), \quad (13)$$

in which we have introduced the dimensionless radial coordinate $\rho_0 = r_0/R$. For any given value of ψ_0, Eqs. 12 and 13 determine ρ_0 and ψ_c. In particular, they together determine the equation $r_0 = R\rho_0(\psi_0)$ of the curve $\mathcal{L}$.

Equations 12 and 13 can be solved simultaneously by first substituting the latter into the former to obtain a single equation giving ψ_c as an implicit function of ψ_0. With $t = \cos\psi_0$ and $T = \cos\psi_c$, this equation can be written in the form:

$$[C^2 + (1 - C^2)T^2][t^2 + T^2(1 - 2t^2) - 2t(1 - t^2)^{1/2}T(1 - T^2)^{1/2}] = \lambda_a^2[C^4t^2 + T^2[1 - (1 + C^4)t^2] - 2C^2t(1 - t^2)^{1/2}T(1 - T^2)^{1/2}]. \quad (14)$$

We settle for a solution of Eq. 14 in the form of the perturbation expansion

$$T = t + \lambda_a T_1 + \lambda_a^2 T_2 + \lambda_a^3 T_3 + \cdots.$$

The zeroth-order approximation $T \sim t$ follows immediately from the fact that, in the limit of vanishing particle size, $\psi_c \sim \psi_0$. By expanding both sides of Eq. 14 in powers of λ_a and equating the coefficients of like powers, one obtains a set of equations which successively determine $T_1, T_2, \ldots$. Expressions for the first two correction terms are as follows:

$$T_1 = \frac{(1 - C^2)t(1 - t^2)}{[C^2 + (1 - C^2)t^2]^{1/2}},$$

$$T_2 = \frac{(1 - C^2)t(1 - t^2)\{2C^2 - (1 - C^2)t^2[C^2 + (1 - C^2)t^2]\}}{2[C^2 + (1 - C^2)t^2]^2}.$$

(Attention is restricted to the first quadrant. Concerning T_1, the perturbation scheme actually yields an expression for T_1^2. The positive square root is chosen because in the first quadrant $\psi_c \le \psi_0$ so $\cos\psi_c \ge \cos\psi_0$.)

A perturbation expansion for ρ_0 is obtained by writing Eq. 13 in terms of t and T, developing the resulting equation in powers of λ_a and utilizing the expressions for T_1 and T_2. This procedure yields:

$$\rho_0 = 1 + \lambda_a(\rho_0)_1 + \lambda_a^2(\rho_0)_2 + O(\lambda_a^3), \quad (15)$$

where

$$(\rho_0)_1 = -[C^2 + (1 - C^2)t^2]^{1/2}, \quad (16)$$

$$(\rho_0)_2 = -\frac{(1 - C^2)^2t^2(1 - t^2)}{2[C^2 + (1 - C^2)t^2]}. \quad (17)$$

Once $\rho_0(\psi_0)$ is known, F_p is given by:

$$F_p = \frac{4}{\pi R^2}\int_0^{\pi/2}\int_0^{R\rho_0(\psi_0)} r_0 dr_0 d\psi_0 = \frac{2}{\pi}\int_0^{\pi/2}[\rho_0(\psi_0)]^2 d\psi_0.$$

Thus, one obtains for the partition coefficient

$$\Phi = \int_0^{\pi/2} F_p \sin\theta d\theta = (2/\pi)\int_0^{\pi/2}\int_0^{\pi/2}[\rho_0(\psi_0)]^2 d\psi_0 \sin\theta d\theta.$$

Substitution of the perturbation expansion (Eq. 15) then leads to the asymptotic formula

$$\Phi = 1 + \Phi_1\lambda_a + \Phi_2\lambda_a^2 + O(\lambda_a^3), \quad (18)$$

where

$$\Phi_1 = (4/\pi)\int_0^{\pi/2}\int_0^{\pi/2}(\rho_0)_1 d\psi_0 \sin\theta d\theta, \quad (19)$$

$$\Phi_2 = (2/\pi)\int_0^{\pi/2}\int_0^{\pi/2}[(\rho_0)_1^2 + 2(\rho_0)_2]d\psi_0 \sin\theta d\theta, \quad (20)$$

in which $(\rho_0)_1$ and $(\rho_0)_2$ are given by Eqs. 16 and 17 with $C = [\cos^2\theta + (b/a)^2\sin^2\theta]^{1/2}$ and $t = \cos\psi_0$.

For a sphere ($a = b$), it can easily be checked that the formulas above give $\Phi_1 = -2$ and $\Phi_2 = 1$, in agreement with Eq. 3 that is well known. The special case of a circular disc is recovered by setting $b/a = 0$, so that $C = |\cos\theta|$. For this case, the integrals in Eqs. 19 and 20 can be evaluated analytically to give

$$\Phi = 1 - (\pi/2)\lambda_a + (1/2)\lambda_a^2 + O(\lambda_a^3) \quad \text{(disc)}. \quad (21)$$

For arbitrary aspect ratios it is found by numerical integration that the first correction given by Eq. 19 agrees with that

which would be calculated via substitution of the expression for the mean projected radius of an oblate spheroid (Giddings et al., 1968) into the asymptotic equation (Eq. 2):

$$\Phi_1 = -2r_m/a = -b/a - [1 - (b/a)^2]^{-1/2} \sin^{-1}\{[1 - (b/a)^2]^{1/2}\} \quad (22)$$

In order to provide a convenient analytical formula, values of Φ_2 determined from Eq. 20 by numerical integration have been fitted with a quadratic polynomial in b/a by the method of least squares:

$$\Phi_2 = 0.489 + 0.279(b/a) + 0.239(b/a)^2. \quad (23)$$

Prolate spheroids

For prolate spheroids, the half axial length b is more appropriate as a characteristic size than the radius a. Therefore, $\lambda_b = b/R$ is used as the perturbation parameter. Starting from Eq. 15, one may show that ρ_0 is given by the expansion:

$$\rho_0 = 1 + \lambda_b\overline{(\rho_0)_1} + \lambda_b^2\overline{(\rho_0)_2} + O(\lambda_b^3), \quad (24)$$

where

$$\overline{(\rho_0)_1} = (a/b)(\rho_0)_1 = -\{\bar{C}^2 + [(a/b)^2 - \bar{C}^2]t^2\}^{1/2}, \quad (25)$$

$$\overline{(\rho_0)_2} = (a/b)^2(\rho_0)_2 = -\frac{[(a/b)^2 - \bar{C}^2]^2 t^2(1 - t^2)}{2\{\bar{C}^2 + [(a/b)^2 - \bar{C}^2]t^2\}}, \quad (26)$$

in which $t = \cos\psi_0$ and

$$\bar{C} = (a/b)C = [\sin^2\theta + (a/b)^2\cos^2\theta]^{1/2}. \quad (27)$$

The partition coefficient is given by Eqs. 18 through 20 with λ_b, $\overline{(\rho_0)_1}$ and $\overline{(\rho_0)_2}$ everywhere replacing, respectively, λ_a, $(\rho_0)_1$, and $(\rho_0)_2$.

As before, values of Φ_1 appearing in the expansion

$$\Phi = 1 + \Phi_1\lambda_b + \Phi_2\lambda_b^2 + O(\lambda_b^3) \quad (28)$$

agree with what would be calculated from Eq. 2 utilizing the mean projected radius of a prolate spheroid (Giddings et al., 1968):

$$\Phi_1 = -2r_m/b = -1 - \frac{(a/b)^2}{[1 - (a/b)^2]^{1/2}} \cdot \ln\left\{\frac{1 + [1 - (a/b)^2]^{1/2}}{(a/b)}\right\}. \quad (29)$$

[Giddings et al. (1968) inadvertently omitted the + within the argument of the logarithm (cf. their Eq. 37). This misprint is corrected in the corresponding formula listed by Baltus and Anderson (1984).] A convenient empirical approximation formula for Φ_2 is

$$\Phi_2 = 0.004 + 0.701(a/b) + 0.291(a/b)^2. \quad (30)$$

It follows from Eqs. 25 and 26 that Φ_2 for a rod ($a/b = 0$) is zero.

Hemispheres

The projection of a hemisphere with radius a is a semicircle with radius a capped by a half-ellipse with major axis a and minor axis $a|\cos\theta|$. It follows that, for any given value of θ, F_p for a hemisphere is one half F_p for the sphere plus one half F_p for the disc of equal radius. Thus, the partition coefficient for a hemisphere in a circular pore is just the arithmetic mean of the corresponding sphere and disc results:

$$\Phi[\text{hemisphere, radius } a] = (1/2)\Phi[\text{sphere, radius } a] + (1/2)\Phi[\text{disc, radius } a]. \quad (31)$$

Combination of Eqs. 3 and 21 yields the asymptotic formula

$$\Phi = 1 - (1 + \pi/4)\lambda_a + (3/4)\lambda_a^2 + O(\lambda_a^3) \text{ (hemisphere)}. \quad (32)$$

Circular cylinders

The projection ($\phi = \pi/2$) of a circular cylinder with radius a and length $2b$ is a rectangle with horizontal and vertical side-lengths $2a$ and $2b\sin\theta$, respectively, capped from above and below by half-ellipses with horizontal and vertical semiaxes a and $a|\cos\theta|$, respectively. The analysis above applied to the special case of a circular disc gives the equation of the curve traced out by the center (r_e, ψ_e) of the upper ellipse. The center of the upper projected ellipse is not, however, the actual center (r_0, ψ_0) of the projection of the cylinder *as a whole*. Further arguments are needed to determine the equation $r_0 = R\rho_0(\psi_0)$ for the curve traced out by the center of the projection of the cylinder. As the preceding developments indicate the general nature of the requisite perturbation analysis, we omit the calculations and simply exhibit the final expressions for the coefficient functions $(\rho_0)_1$ and $(\rho_0)_2$ corresponding to Eqs. 16 and 17:

$$(\rho_0)_1 = -[C^2 + (1 - C^2)t^2]^{1/2} - (b/a)(1 - C^2)^{1/2}(1 - t^2)^{1/2}, \quad (33)$$

$$(\rho_0)_2 = -\frac{(1 - C^2)^2 t^2(1 - t^2)}{2[C^2 + (1 - C^2)t^2]} + (b/a) \cdot \frac{(1 - C^2)^{3/2}t^2(1 - t^2)^{1/2}}{[C^2 + (1 - C^2)t^2]^{1/2}} - (b/a)^2(1 - C^2)t^2/2, \quad (34)$$

with $C = |\cos\theta|$ and $t = \cos\psi_0$. These expressions lead to the final result:

$$\Phi = 1 - [\pi/2 + (b/a)]\lambda_a + [1/2 + (b/a)]\lambda_a^2 + O(\lambda_a^3) \text{ (circular cylinder)}. \quad (35)$$

This formula is suitable for taking the limit $(b/a) \to 0$. As in the case of prolate spheroids, for $(b/a) > 1$ it is advantageous to rewrite Eq. 35 as an expansion in $\lambda_b = b/R$ so that one can recover the limiting case of an infinitesimally thin rod.

Asymptotic Formulas vs. Simulation Results

Values of the partition coefficient calculated using the asymptotic formulas derived above are compared with simulation results in Figure 9. Good agreement is apparent even at rather large values of the ratio λ_a or λ_b of molecule size to pore

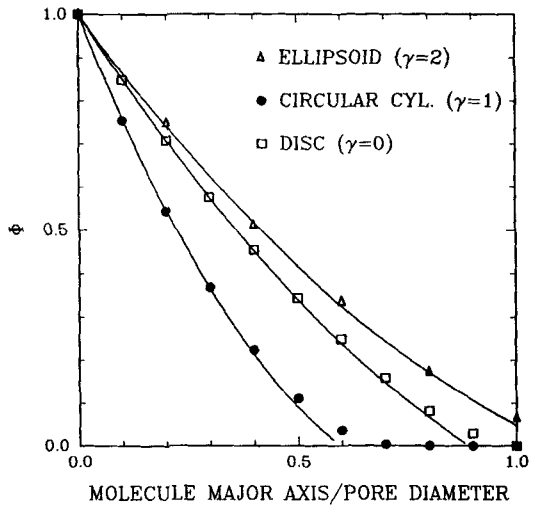

Figure 9. Comparison of perturbation analysis, given as lines, and Monte Carlo results, given as points, for various molecule shapes in circular pores.

radius. The asymptotic formulas give accurate predictions except when Φ is small. This is remarkable in view of the fact that these formulas were derived using a boundary perturbation analysis for the case $\lambda \ll 1$, which *a priori* would seem to require that Φ be close to unity.

Pores of Nonuniform Cross-Section

Pores of uniform cross-section are desirable for use in experiments that characterize the diffusion of large molecules (Deen, 1987). For such experiments, the results presented above are directly applicable. Uniform pores also serve as simple models of the intricately-shaped void space in actual porous materials. Unfortunately, the connection between model and reality is more tenuous in such cases. It is, therefore, of value to consider additional pore models that more accurately represent various types of tortuous microstructure.

In this section we consider partitioning of spherical and rod-shaped molecules within the cavity between sinusoidally corrugated plates, and spherical molecule partitioning in the interstitial space within both cubic arrays of touching spheres and periodic arrays of circular fibers.

As in the case of uniform pores, the initial effects of increasing molecule size conform to the asymptotic behavior described by Eq. 2. Pore wall curvature and details of molecule shape are responsible for higher-order terms, which become important at larger values of λ.

Sinusoidally corrugated plates

Consider the pore bounded by two sinusoidally corrugated plates. This geometry leads to several parameters that characterize the pore size and shape, including the mean plate separation, the amplitude of the corrugations, and the wavelength of the corrugations. Further complexities could be introduced by altering the phase shift between the top and bottom corrugations or by allowing corrugations in a single pore to have different amplitudes and wavelengths, although such problems are not addressed here.

An important feature of nonuniform pores is the appearance of a molecule cutoff size. Molecules which might fit in the body of a pore will be excluded from passing through the throat of a pore when their smallest linear dimension exceeds the width of the throat. We term this point of exclusion the molecule cutoff size. Figure 10 describes the partitioning, as determined by Monte Carlo simulation, of spherical and rod-shaped molecules in a sinusoidal-plate pore of mean separation distance 0.5, corrugation wavelength 1, and corrugation amplitude 0.125. The infinitely thin rod-shaped molecules may always find an orientation which allows them to pass through this pore. Spherical molecules, however, will be blocked from passing axially along the pore when a molecule cutoff diameter of 0.25 is reached. If we consider molecules which travel perpendicular to the corrugations in an infinitely long pore, Φ will vanish when the molecule cutoff size is reached, resulting in a discontinuity in the partitioning curve. The rate of diffusion through such pores will not, however, exhibit such a discontinuity since an increase in hydrodynamic resistance will force the effective diffusivity to smoothly approach zero. Interestingly, the portion of the partitioning curve to the right of the cutoff does have physical significance in this case. It describes partitioning for transport in the direction parallel to corrugations.

Figure 11 describes the effect of corrugation amplitude on partitioning of rod-shaped molecules. Partitioning decreases at large λ because very long thin molecules are effectively constrained by the closest approach of pore walls. As corrugation amplitude is increased, the dominant effect is a decrease in closest approach of the pore walls which reduces the partition coefficient. With a relatively long corrugation wavelength, such as that used for Figure 11, spherical molecules would not experience this reduction in the partition coefficient because they would not span from one pore throat to the next. For spheres and short rods, the partition coefficient will increase due to pore wall curvature and the partial exclusion of molecules from narrow portions of the pore. These effects of pore wall curvature are discussed in detail in the section below on fibrous networks.

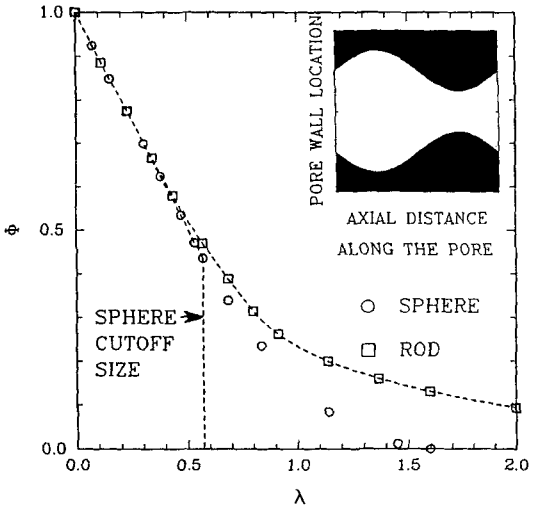

Figure 10. Comparison of spherical and rod-shaped molecule partitioning in sinusoidal parallel plate pores.

Mean separation of plates = 0.5, wavelength = 1, and amplitude = 0.125.

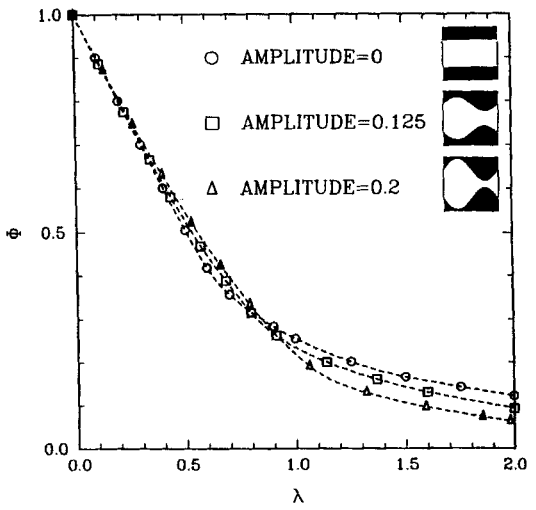

Figure 11. Effect of corrugation amplitude on partitioning of rod-shaped molecules in sinusoidal parallel plate pores.

Mean separation of plates = 0.5 and wavelength = 1.

Figure 12 describes the effect of corrugation wavelength on rod-shaped molecule partitioning. For a molecule of given size, the partition coefficient will become increasingly insensitive to changes in corrugation wavelength as the wavelength decreases. The surface area of the pore, however, will increase relative to the molecule size and pore volume. These combined effects increase λ while only slightly decreasing Φ, thus shifting the partitioning curve to the right. When the pore walls become extremely tortuous λ is no longer an appropriate-size parameter for large molecules because these molecules rarely penetrate into the pore wall crevices. A similar phenomenon is demonstrated in Figure 5 for rectilinear pores in that λ loses significance as a universal-size parameter when a crucial pore dimension is of the same order of magnitude or smaller than the maximum linear dimension of the molecule.

Partitioning in granular materials

Granular materials, such as some catalysts and chromatographic packings, are modeled as simple cubic (SC), body centered cubic (BCC), and face centered cubic (FCC) lattices of touching spherical grains. The void fraction of these lattices ranges from 0.26 for FCC to 0.48 for SC.

Figure 13 compares the partition coefficient for spherical molecules in these three lattice frameworks. The fact that partitioning in these lattices is not a strong function of void fraction is encouraging because it suggests that partitioning in granular materials might be estimated in practice by an equivalent rectilinear pore model. Even at appreciable values of λ, an equivalent circular pore represents these partitioning curves well, especially that of the FCC lattice. Small molecule partitioning in granular materials could be accurately calculated if the void fraction and surface area were known. Large molecule partitioning could be estimated if the molecule cutoff size and particulars of grain morphology were known.

Partitioning in fibrous networks

Partitioning in sparse fibrous networks differs from that of the previous cases discussed in that fibrous pores may have a "predominantly convex" pore wall curvature. When the pore wall is "predominantly convex," the partitioning curve has a negative second derivative, $d^2\Phi/d\lambda^2$, as opposed to a positive second derivative for concave pores. This phenomenon is evident in a formula derived by Ogsten (1958) for random fibrous networks and was observed experimentally in a sephadex gel by Laurent and Killander (1964).

To clarify this behavior we consider three cases: the pore space between two parallel plates; the pore space inside of a cylindrical duct; and the pore space outside of a single cylindrical fiber. The parallel-plate pore has no curvature and therefore partitioning behavior of spherical molecules may be described by Eq. 2. The cylindrical duct has concave pore wall curvature. The pore volume excluded to a spherical molecule is, therefore, smaller than that excluded to the same molecule in an equivalent parallel-plate pore. As a result, leading order effects embodied in Eq. 2 will underestimate Φ. The cylindrical fiber has convex pore walls. The excluded volume is therefore greater than that for an equivalent flat wall and Eq. 2 will overestimate Φ.

Despite the fact that the surface of a cylindrical fiber is convex, the pore wall curvature in fibrous materials may be "predominantly concave." When fibers touch or come sufficiently close to one another, the steric exclusion layers individually associated with each fiber will overlap. This reduces the total pore volume excluded to molecules and consequently increases Φ. When the pore volume excluded to molecules is less than that of an equivalent parallel-plate pore, we consider the pore walls to be "predominantly concave" in nature.

Fibrous materials can be quite sparse. The general morphology and rigidity of fibers allow them to be largely free-standing (not touching each other). When fibers are sufficiently separated from one another, the pore wall curvature will be "convex" for all but large molecules which may touch two or more fibers at one time.

Spherical molecule partitioning in periodic crossed fiber networks was determined by Monte Carlo simulation. The unit cells shown in Figure 14 were used in all simulations and the

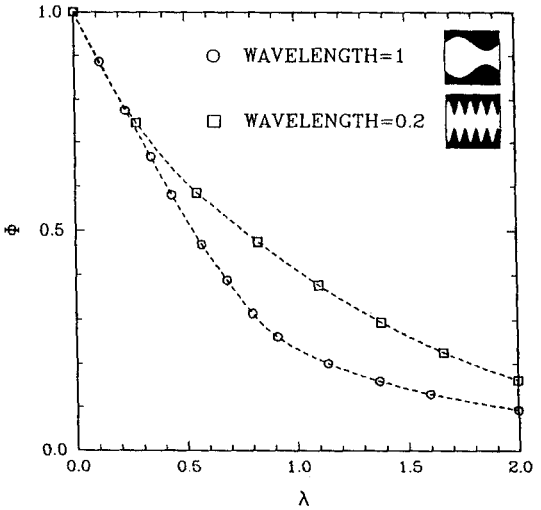

Figure 12. Effect of corrugation wavelength on partitioning of rod-shaped molecules in sinusoidal parallel plate pores.

Mean separation of plates = 0.5 and amplitude = 0.125.

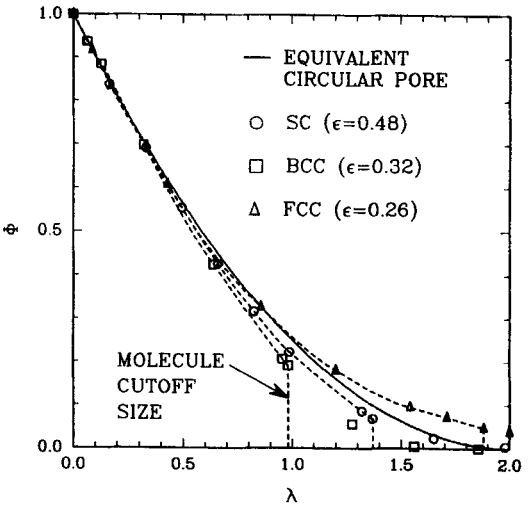

Figure 13. Comparison of spherical molecule partitioning in simple cubic (SC), body centered cubic (BCC), and face centered cubic (FCC) lattices of spherical grains.

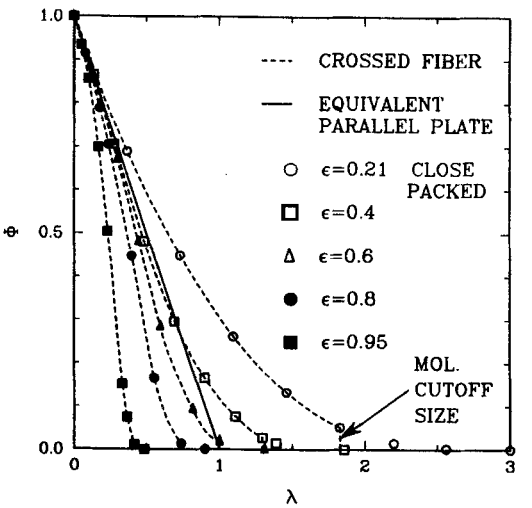

Figure 15. Effect of void fraction ϵ on spherical molecule partitioning in crossed fiber porous networks.

fibrous network porosity, ϵ, was varied by altering the fiber radius. Results are given in Figure 15 with the upper limit for crossed fibers being the close packed fiber case with an ϵ of 0.21. In the case of close packed fibers, the pore appears concave because the close proximity of fibers results in overlap of molecular exclusion layers. The resulting partitioning curve is consequently above that of the equivalent parallel-plate case representative of no pore wall curvature. As the fibers radius is decreased, the fibers become more separated and eventually appear "convex" to all but very large molecules. The partitioning curve therefore has a negative second derivative, $d^2\Phi/d\lambda^2$, at small λ and a positive second derivative after the molecule becomes large enough to touch two fibers at once. Since the relative space between the fibers considered increases as fiber radius is decreased, the partitioning curve becomes steeper as the porosity ϵ is increased.

All of the Monte Carlo results plotted in Figure 15 have mathematical significance as a ratio of the configurational integrals, Eq. 4. Points to the right of the molecular cutoff size might also have physical significance if lattice imperfections existed which would allow larger molecules to enter the lattice.

The partitioning characteristics of fibrous networks lend insight into certain features of the other pore models considered above. The predominant pore wall curvature in granular materials, for instance, is "concave" because of the close proximity of grains. The structural integrity of granular materials requires that each grain touch its neighbors at a number of points (Batchelor and O'Brien, 1977, p. 330). The contact of grains introduces an overall concavity to the pore due to the overlap of molecular exclusion layers.

Sinusoidal pores possess alternating pore wall regions respectively identifiable as "convex" and "concave." The partition coefficient for a spherical molecule will be equal to or greater than that for the equivalent parallel-plate pore. When steric exclusion layers independently associated with the top and bottom plates overlap, spheres and short rods will be preferentially excluded from the narrow "convex" regions of the pore. In this case, the molecule will "see" mostly concave pore walls. This explains the increase of Φ with amplitude at small λ evident in Figure 11.

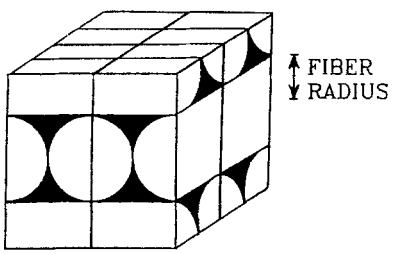

Figure 14. Crossed fiber unit cells.

Notation

a = radius of axisymmetric molecule
b = half axial length of axisymmetric molecule
C = ratio of semiaxes of molecule projections
E = elliptic integral of the second kind
f = function describing elliptical projection of molecule
F = elliptic integral of the first kind
F_p = fraction of pore cross-sectional area accessible to molecule center at a given molecule orientation
h = closest approach of a molecule center to a flat surface at a given molecule orientation
$\mathcal{L}$ = curve bounding the set of positions accessible to molecule center at a given molecule orientation
$P(\underline{x}, \underline{\phi})$ = probability density of the molecule having configuration $(\underline{x}, \underline{\phi})$
r = radial polar coordinate
R = radius of circular cylindrical pore
r_m = mean projected radius of molecule as described in Eq. 1
r_o = radial polar coordinate of molecule center
t = cos (ψ_o)
T = cos (ψ_c)
$(V/S)_p$ = hydraulic radius of porous medium, the ratio of pore volume to surface area
$\underline{x}$ = position of molecule center

Greek letters

α = dimensionless radial coordinate used in Eq. 7
γ = molecule aspect ratio, b/a
θ = polar angle between pore and molecule axes

λ = ratio of molecule to pore size expressed as $r_m/(V/S)_p$
λ_a = ratio of molecule radius to circular pore radius, a/R
λ_b = ratio of molecule half length to circular pore radius, b/R
ρ_o = dimensionless radial polar coordinate of molecule center
$(\rho_o)_1$, $(\rho_o)_2$ = coefficient functions used in perturbation expansion for ρ_o
ϕ = azimuthal angle specifying molecule orientation
$\underline{\phi}$ = set of angles describing molecule orientation
Φ = partition coefficient
Φ_1, Φ_2 = coefficients in perturbation expansion for Φ
ψ = angular polar coordinate
ψ_o = angular polar coordinate of molecule center
ψ_c = angular polar coordinate of point of contact between molecule and circular pore boundary

Literature Cited

Anderson, J. L., "Configurational Effect on the Reflection Coefficient for Rigid Solutes in Capillary Pores," *J. Theor. Biol.*, **90,** 405 (1981).

Anderson, J. L., and D. M. Malone, "Mechanism of Osmotic Flow in Porous Membranes," *Biophys. J.*, **14,** 957 (1974).

Anderson, J. L., and J. A. Quinn, "Restricted Transport in Small Pores: A Model for Steric Exclusion and Hindered Particle Motion," *Biophys. J.*, **14,** 130 (1974).

Baltus, R. E., and J. L. Anderson, "Hindered Diffusion of Asphaltenes Through Microporous Membranes," *Chem. Eng. Sci.*, **38,** 1959 (1983).

———, "Comparison of G.P.C. Elution Characteristics and Diffusion Coefficients of Asphaltenes," *Fuel*, **63,** 530 (1984).

Batchelor, G. K., and R. W. O'Brien, "Thermal or Electrical Conduction through a Granular Material," *Proc. Roy. Soc.*, (London), **A355,** 313 (1977).

Brenner, H., and L. J. Gaydos, "The Constrained Brownian Movement of Spherical Particles in Cylindrical Pores of Comparable Radius," *J. Colloid Interf. Sci.*, **58,** 312 (1977).

Cheng, W., "Surface Exclusion and Geometrical Exclusion," *J. Chromatog.*, **362,** 309 (1986).

Davidson, M. G., U. W. Suter, and W. M. Deen, "Equilibrium Partitioning of Flexible Macromolecules between Bulk Solution and Cylindrical Pores," *Macromolec.*, **20,** 1141 (1987).

Deen, W. M., "Hindered Transport of Large Molecules in Liquid-Filled Pores," *AIChE J.*, **33,** 1409 (Sept., 1987).

Ferry, J. D., "Statistical Evaluation of Sieve Constants in Ultrafiltration," *J. Gen. Physiol.*, **20,** 95 (1936).

Giddings, J. C., E. Kucera, C. P. Russell, and M. N. Myers, "Statistical Theory for the Equilibrium Distribution of Rigid Molecules in Inert Porous Networks. Exclusion Chromatography," *J. Phys. Chem.*, **72,** 4397 (1968).

Glandt, E. D., "Noncircular Pores in Model Membranes: A Calculation of the Effect of Pore Geometry on the Partition of Solute," *J. Memb. Sci.*, **8,** 331 (1981).

Laurent, T. C., and J. Killander, "A Theory of Gel Filtration and Its Experimental Verification," *J. Chromatog.*, **14,** 317 (1964).

Malone, D. M., and J. L. Anderson, " Hindered Diffusion of Particles Through Small Pores," *Chem. Eng. Sci.*, **33,** 1429 (1978).

Ogston, A. G., "The Spaces in a Uniform Random Suspension of Fibers," *Trans. Farad. Soc.*, **54,** 1754 (1958).

Pappenheimer, J. R., E. M. Renkin, and L. M. Borrero, "Filtration, Diffusion and Molecular Sieving Through Peripheral Capillary Membranes: A Contribution to the Pore Theory of Capillary Permeability," *Am. J. Physiol.*, **167,** 13 (1951).

Porath, J., "Some Recently Developed Fractionation Procedures and Their Application to Peptide and Protein Hormones," *Pure and Appl. Chem.*, **6,** 233 (1963).

Renkin, E. M., "Filtration, Diffusion, and Molecular Sieving through Porous Cellulose Membranes," *J. Gen. Physiol.*, **38,** 225 (1954).

Rikvold, P. A., and G. Stell, "D-Dimensional Interpenetrable-Sphere Models of Random Two-Phase Media: Microstructure and an Application to Chromatography," *J. Colloid Interf. Sci.*, **108,** 158 (1985).

Satterfield, C. N., C. K. Colton, and W. H. Pitcher, "Restricted Diffusion in Liquids within Fine Pores," *AIChE J.*, **19,** 628 (Aug., 1973).

Smith, III, F. G., and W. M. Deen, "Electostatic Effects on the Partitioning of Spherical Colloids between Dilute Bulk Solution and Cylindrical Pores," *J. Colloid Interf. Sci.*, **91,** 571 (1983).

Solomon, A. K., "Characterization of Biological Membranes by Equivalent Pores," *J. Gen. Physiol.*, **51,** 335s (1968).

Van Kreveld, M. E., and N. van den Hoed, "Mechanism of Gel Permeation Chromatography: Distribution Coefficient," *J. Chromatog.*, **83,** 111 (1973).

Manuscript received June 20, 1988 and revision received Sept. 7, 1988.